東北大学機関リポジトリ
TOUR
Tohoku University Repository

Electronic properties across metal-insulator transition in β-pyrochlore-type CsW2O6 epitaxial films

著者	Takuto Soma, Kohei Yoshimatsu, Koji Horiba, Hiroshi Kumigashira, Akira Ohtomo
journal or publication title	Physical Review Materials
volume	2
number	115003
page range	1-8
year	2018-11-27
URL	http://hdl.handle.net/10097/00125547

doi: 10.1103/PhysRevMaterials.2.115003

Electronic properties across metal-insulator transition in β-pyrochlore-type CsW_2O_6 epitaxial films

Takuto Soma,[1] Kohei Yoshimatsu,[1,*] Koji Horiba,[2,3] Hiroshi Kumigashira,[2,3] and Akira Ohtomo[1,3]

[1]*Department of Chemical Science and Engineering, Tokyo Institute of Technology, 2-12-1 Ookayama, Meguro-ku, Tokyo 152–8552, Japan*

[2]*Photon Factory, Institute of Materials Structure Science, High Energy Accelerator Research Organization (KEK), 1-1 Oho, Tsukuba 305–0801, Japan*

[3]*Materials Research Center for Element Strategy (MCES), Tokyo Institute of Technology, Yokohama 226–8503, Japan*

(Received 1 July 2018; revised manuscript received 24 October 2018; published 27 November 2018)

In CsW_2O_6, which undergoes a metal-insulator transition (MIT) at 213 K, the emergence of exotic properties associated with rattling motion of Cs is expected owing to its characteristic β-pyrochlore-type structure. However, a hurdle for crystal growth hampers elucidation of detailed properties and mechanisms of the MIT. Here we report on the epitaxial growth of β-pyrochlore-type CsW_2O_6 films and their electronic properties across the MIT. Using pulsed-laser deposition technique, we grew single-crystalline CsW_2O_6 films exhibiting remarkably lower resistivity compared with a polycrystalline bulk and sharp MIT around 200 K. Negative magnetoresistance and a positive Hall coefficient were found, which became pronounced below 200 K. The valence-band and core-level photoemission spectra indicated the drastic changes across the MIT. In the valence-band photoemission spectrum, the finite density of states was observed at the Fermi level in the metallic phase. In contrast, an energy gap appeared in the insulating phase. The split of W 4f core-level spectrum suggested the charge disproportionation of W^{5+} and W^{6+} in the insulating phase. The change of spectral shape in the Cs 4d core levels reflected the rattling motion of Cs^+ cations. These results strongly suggest that CsW_2O_6 is an exotic material in which MIT is driven by the charge disproportionation associated with the rattling motion.

DOI: 10.1103/PhysRevMaterials.2.115003

I. INTRODUCTION

β-pyrochlore-type oxides (AM_2O_6) have recently attracted much attention as they show anomalous phonon induced properties [1–4]. β-pyrochlore is also known as defect-type pyrochlore, where the A cations are large enough to share space with oxygen [5]. The crystal structures of normal and β-pyrochlore-type oxides are schematically shown in Fig. 1. In contrast to the normal pyrochlore with relatively small A' cations ($A'_2M_2O_7$) [Fig. 1(a)], A cations occupy O-absent space inside vast cages surrounded by the octahedral MO_6 framework, leaving the original A'-site entirely empty [Fig. 1(b)]. As a result, anomalous local atomic vibration of the A cations called rattling is realized, which is also illustrated in Fig. 1(b) [1–4]. The rattling phonon is responsible for strong electron-phonon interaction and low thermal conductivity, which trigger exotic properties such as superconductivity and high thermoelectric effects [4,6,7].

Among β-pyrochlore-type oxides, $AOs_2O_6 (A = K, Rb, Cs)$ have been actively investigated. Preparation of high-quality single crystals is possible and various properties have been elucidated [2–4]. For example, AOs_2O_6 show superconductivity associated with the rattling motion of the A cations and their superconducting transition temperature varies in accordance with the A atoms. Except for the osmates, CsW_2O_6 is the only example of β-pyrochlore-type oxides having d electrons, which was synthesized by Cava *et al.* in 1993 [8]. In addition, it is the only example of pyrochlore-type tungstate having d electrons regardless of normal or β-pyrochlore. However, CsW_2O_6 is thermally unstable so that with using conventional synthesis methods even a dense polycrystalline sample cannot be prepared, much less a single crystal [8,9]. Thus, little is known about the physical properties. In 2013, Hirai *et al.* reported that the metal-insulator transition (MIT) occurred at 213 K accompanied by a structural transition (cubic to orthorhombic), and a small magnetization was suddenly quenched in the insulating phase [9]. As they pointed out, the sample quality affected the physical properties. Furthermore, magnetotransport and electron spectroscopy experiments have not been carried outyet. Thus, it has been enthusiastically desired to reveal the intrinsic properties of CsW_2O_6 in viewpoints of understanding not only a class of β-pyrochlore-type oxide, but also an analogue to 5d pyrochlore $A_2Ir_2O_7$ (A is lanthanides), which exhibits topological states owing to strong spin-orbit coupling [10–13].

In this paper, we have fabricated β-pyrochlore-type CsW_2O_6 epitaxial films to investigate their electronic properties in detail. Using the pulsed-laser deposition (PLD) technique, high-quality single-crystalline CsW_2O_6 films were successfully grown on lattice-matched Y-stabilized ZrO_2 (YSZ) substrates. The temperature dependence of resistivity indicated the clear MIT around 200 K. From magnetotransport measurements, negative magnetoresistance was observed in lower and higher temperatures near the MIT. Synchrotron-radiation photoemission measurements were performed at temperatures over the MIT. The valence-band spectra

*Author to whom correspondence should be addressed: k-yoshi@apc.titech.ac.jp

 ©2018 American Physical Society

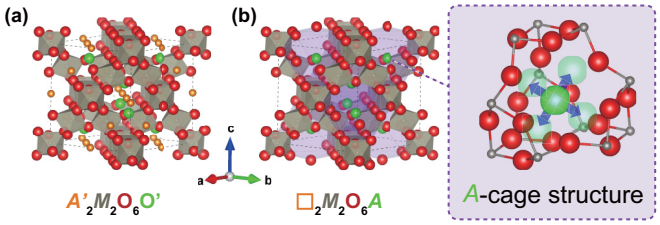

FIG. 1. Schematics of the crystal structures of (a) normal pyrochlore-type $A'_2M_2O_7$ and (b) β-pyrochlore-type AM_2O_6 and its A-cage structure. Note that the locations of O′ in (a) and A atoms in (b) are identical to each other.

reflected a gap near the Fermi level (E_F) in the insulating phase. The W 4f core levels evolved their spectral shape and two components were discriminated in the insulating phase, being consistent with charge disproportionation of W^{5+} and W^{6+} states. The Cs 4d core-level spectra drastically changed across the MIT, reflecting the rattling motion of Cs^+ cations. These results suggest that the MIT of CsW_2O_6 originates from the charge disproportionation of W cations and the rattling motion of Cs^+ cations.

II. EXPERIMENT

CsW_2O_6 films were grown on YSZ (111) substrates by using the PLD technique with a KrF excimer laser (0.6 J cm^{-2}, 6 Hz). A $CsW_2O_{6+\delta}$ ceramic tablet as a laser-ablation target was prepared by conventional solid-state reaction steps, starting from mixture of Cs_2CO_3 and WO_3 powders with a stoichiometric molar ratio (Cs:W = 1:2). Generally, for compounds containing alkali metals, the adjustment of film stoichiometry is often difficult in PLD growth due to high vapor pressure of alkali metals [14]. For the present Cs-W-O system, however, stoichiometric transfer of cation compositions from targets to films has been revealed by electron probe microanalyzer in our previous study [15]. The substrate temperature and oxygen pressure (P_{O2}) were set to 650 °C and 7.5 mTorr, respectively, while pure oxygen (6 N purity) was fed into a vacuum chamber during the growth. The film thickness ranged from 30 to 200 nm, as verified by a stylus-type profiler. Most of the properties were measured for ∼150-nm-thick films.

The structural properties were investigated by a laboratory x-ray diffraction (XRD) apparatus with Cu Kα_1 radiation. The temperature dependence of resistivity and magnetoresistance were measured by a standard four-probe method using a physical property measurement system (Quantum Design, PPMS). The magnetic field was applied perpendicular to film surface. All of the temperature dependence of magnetotoransport measurements were performed in a zero-field cooling process. Consequently, the field was swept from 0 T. Ti/Au metal electrodes were vacuum-evaporated on the films for electrical ohmic contacts.

Photoemission spectroscopy (PES) was performed for samples transferred *ex situ* at the undulator beamline of BL-2A in the Photon Factory, KEK. The PES spectra were recorded using an electron energy analyzer (SES-2002, VG Scienta) with an energy resolution of less than 150 meV at

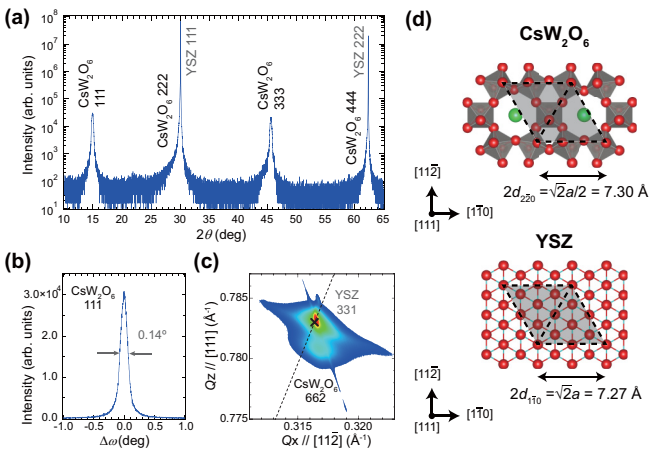

FIG. 2. (a) Typical out-of-plane XRD pattern for CsW_2O_6 films on YSZ (111) substrates grown under the optimized condition. (b) ω scan for the CsW_2O_6 111 reflection. (c) Reciprocal space map around the YSZ 331 reflection. The reciprocal point of bulk CsW_2O_6 662 reflection is indicated by crossing bars. The broken line intersects the axis origin. (d) Schematics of crystal structures of CsW_2O_6 and YSZ projected along [111] directions. The red and green spheres indicate oxygen and Cs atoms, respectively. The hatched areas surrounded by broken lines represent the surface unit cells for epitaxial growth.

phonon energy of 630 eV at RT. E_F was referred to that of Au electrically in contact with the sample surface.

III. RESULTS AND DISCUSSION

We first describe the structural properties of a single-crystalline CsW_2O_6 epitaxial film. Figure 2(a) shows the out-of-plane XRD pattern of the CsW_2O_6 film. Only β-pyrochlore-type CsW_2O_6 odd hhh reflections were detected along YSZ 111 and 222 reflections, indicating (111)-oriented CsW_2O_6 films. CsW_2O_6 even hhh reflections were hardly discriminated from the substrate reflections due to their close lattice constants to each other [16]. We note that the lattice constants of normal pyrochlore-type structure are comparable to those of the β- pyrochlore-type one. However, the formation of β-pyrochlore-type structure was evidenced by the strong 111 reflection with respect to other reflections [17]. As shown in Fig. 2(b), the full width at half maximum (FWHM) of the ω scan of the CsW_2O_6 111 reflection was 0.14°, indicating high in-plane lattice coherency. To investigate further details about the in-plane lattice structures, we also took reciprocal space map around the YSZ 331 reflection as shown in Fig. 2(c). The in-plane epitaxial relationship was verified as $CsW_2O_6[1\bar{1}0] \parallel YSZ[1\bar{1}0]$. Note that this epitaxial relationship is identical to that of normal pyrochlore-type iridate films grown on YSZ (111) substrates [18,19]. In addition, Q_x values between the film and substrate were identical, indicating that CsW_2O_6 films were coherently grown on the YSZ lattice.

Figure 2(d) illustrates epitaxial relationship between CsW_2O_6 and YSZ projected along the [111] direction. The double $d_{2\bar{2}0}$ spacing of CsW_2O_6 (7.30 Å) is close to double $d_{1\bar{1}0}$ spacing of YSZ (7.27 Å), and their mismatch is only 0.4% [9]. Therefore, high-quality single-crystal CsW_2O_6 films could be grown on the lattice matched substrates. We

would like to emphasize that this is the first demonstration of epitaxial growth of β-pyrochlore-type compounds. We also note that CsW_2O_6 bulk obtained previously are low-dense polycrystals, but not single crystals [8,9]. The nonequilibrium thin-film synthesis and excellent lattice matching to the YSZ substrate realizes epitaxial stabilization of the metastable β-pyrochlore phase.

Next, we describe transport properties of the CsW_2O_6 film. Figure 3(a) shows the temperature dependence of resistivity ρ for the CsW_2O_6 film. For comparison, we also plotted the ρ-T curve of low-dense polycrystalline bulk CsW_2O_6 [9]. The room-temperature ρ of our film was $\sim 10^{-2}\,\Omega\,\mathrm{cm}$, which was lower by two orders of magnitude than that of bulk. The lower ρ is certainly attributed to the high quality of the samples. Below 200 K, resistivity indicated sharp increase with narrow hysteresis, which was also found in bulk and thought to be the sign of the MIT accompanying the reduction of the structural symmetry [9]. The existence of the hysteresis implies the occurrence of the charge disproportionation as is reported in various mixed-valent compounds, which will be discussed in connection with core-level measurements later [20]. The slight difference in transition temperature (200 K in our film and 213 K in bulk) can be attributed to epitaxial strain and/or slight off-stoichiometry as reported for various compounds exhibiting the MIT [21–23].

In a previous study for bulk, high-temperature (HT) phase ($T > 213\,\mathrm{K}$) has an insulating behavior ($\mathrm{d}\rho/\mathrm{d}T < 0$). Nevertheless, it is assigned to be metallic, and the opposite $\mathrm{d}\rho/\mathrm{d}T$ sign is ascribed to low quality that hinders the intrinsic properties [9]. On the other hand, our film also showed an insulating behavior despite high crystalline quality (FWHM $\sim 0.14^\circ$). This fact suggests that bad metallicity in the HT phase is intrinsic to CsW_2O_6. It should be mentioned that although the crystal quality was independent of film thickness, the MIT disappeared and the insulating behavior appeared in all temperatures when film thickness was reduced down to several tens of nanometers. This is a typical behavior of ultrathin films of transition-metal oxides [24–26].

In the low-temperature (LT) phase, the conduction mechanism was different from the previous reports. In Ref. [13], ρ-T in a LT range is described with thermally activated conduction: $\rho(T) = \rho_0 \exp(E_a/k_B T)$, where ρ_0 is the preexponential term, E_a is activation energy, and k_B is Boltzmann's constant.

In contrast, the LT transport properties of our film were better described with three-dimensional variable-range hopping (VRH) conduction: $\rho(T) = \rho_0 \exp(T_0/T)^{1/4}$, where T_0 is a characteristic temperature representing the strength of carrier localization [27]. Figures 3(b) and 3(c) show a plot of $\ln \rho$ as a function of T^{-1} and $T^{-1/4}$ and corresponding linear fits with thermal activation and VRH models, respectively. In the LT region, the variation of each $\ln \rho$ was linear but gradually deviated from the fitted lines with increasing temperature. The deviation started around 150 K for the thermal activation model [Fig. 3(b)], while around 175 K for the VRH model [Fig. 3(c)]. These results suggest that the carrier conduction mechanism of the LT phase is governed by VRH associated with carrier localization at the W sites. The temperature dependence of Hall coefficient R_H supported the carrier localization in the LT phase as will be discussed later.

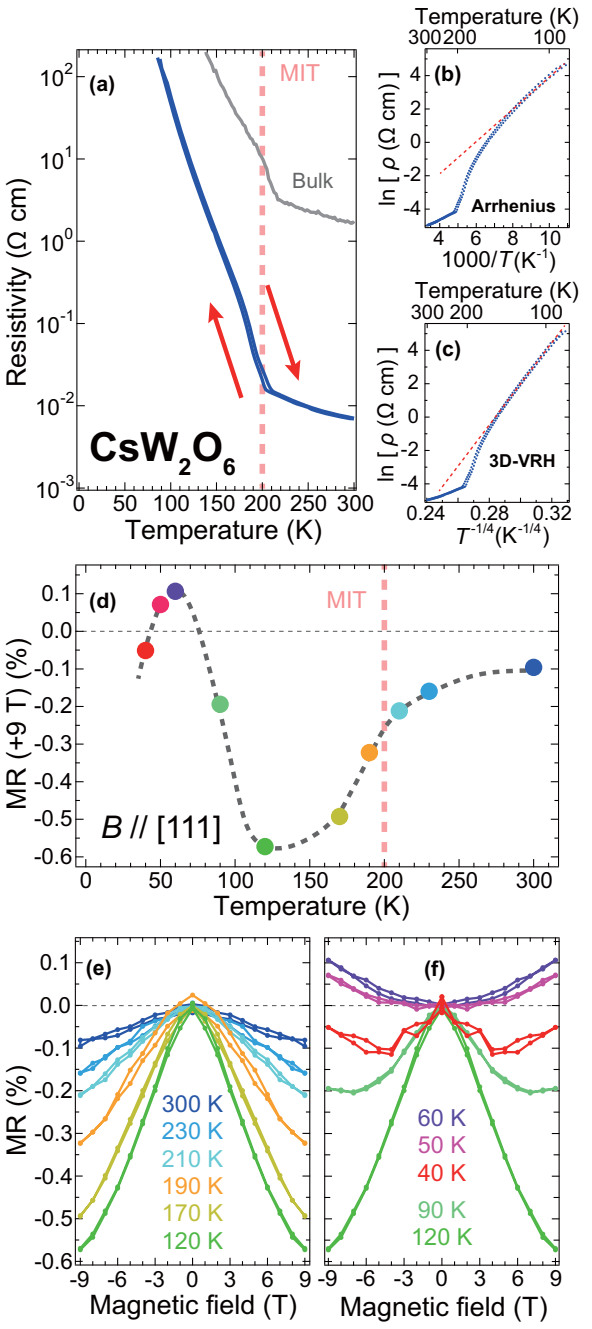

FIG. 3. (a) Temperature dependence of the resistivity for the CsW_2O_6 film. The bulk data are also plotted as a reference [9]. Red arrows and broken lines represent the direction of the temperature sweep and the transition temperature for the film, respectively. (b) $\ln \rho$ vs $1000/T$. The broken line is a linear fit to thermal activation model. (c) $\ln \rho$ vs $T^{-1/4}$. The broken line is a linear fit to the VRH model. (d) Temperature dependence of the magnetoresistance for the CsW_2O_6 film under 9 T. The gray broken line indicates a guide to the eye. (e) and (f) Magnetic field dependence of the magnetoresistance taken at different temperature ranges.

The magnetoresistance (MR) showed intriguing behavior across MIT and repeated sign reversal below 100 K. Figure 3(d) shows the temperature dependence of MR of the CsW_2O_6 film taken at $H = 9\,\mathrm{T}$, where $\mathrm{MR}(H)$ is defined as

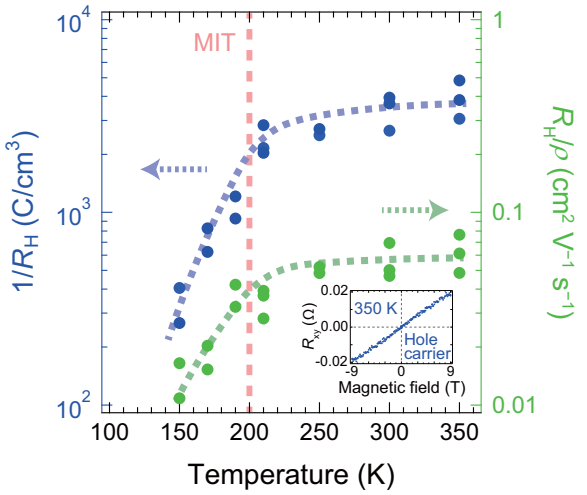

FIG. 4. Temperature dependence of inverse Hall coefficient and Hall mobility. The blue and green broken lines and pink broken line indicate a guide to the eye and the transition temperature, respectively. The inset shows the magnetic field dependence of Hall resistance (R_{xy}) taken at 350 K.

$[\rho(H) - \rho(0)]/\rho(0)$. We subtracted odd function components from raw longitudinal ρ data to obtain MR being an even function of H. The magnetic field dependence of MR taken at various temperatures are shown in Figs. 3(e) and 3(f). The negative MR was observed in a range of 120 K $\leqslant T \leqslant$ 300 K, where the degree of MR modulated across the MIT. The larger signal of negative MR below 200 K suggests the enhancement of the magnetic interaction in the LT insulating phase. A similar negative correlation between the degree of MR and magnetization is generally observed for MIT materials [28]. On the other hand, finite negative MR was found even in the HT phase of our sample, implying that magnetic interaction still remained in the HT phase. In Ref. [9], the HT (LT) phase is considered as a paramagnetic metal (a nonmagnetic insulator). However, our results strongly suggest that both LT and HT phases near MIT are neither nonmagnetic nor paramagnetic.

At temperatures below 100 K, MR indicated anomalous sign reversal. As shown in Fig. 3(f), the negative component gradually decreased with lowering temperature and disappeared around 60 K, where only positive MR with parabolic magnetic field dependence was found. In addition, the negative component revived at 40 K, implying another transition within the LT phase.

Taking a half electron per W site and the indication of magnetic interactions into account, it is relevant to investigate characteristics of mobile charge carriers. The positive Hall coefficient R_H with the linear slope as a function H was revealed, as shown in the inset of Fig. 4 (taken at 350 K), and the same tendencies were found down to 100 K. The number of the Hall carriers in a simple band picture was ~ 2 holes per W atom at 350 K, which was inconsistent with the 0.5 electron per W atom. This result suggests that CsW_2O_6 has a complex multiband structure in correlated metallic states. Figure 4 shows the temperature dependence of inverse R_H. The inverse R_H suddenly decreased below 200 K, which was consistent with MIT. In contrast, the inverse R_H in the HT phase was independent of temperature, which was also consistent with metallic nature. Apparent Hall mobility R_H/ρ was $\sim 0.06\,\mathrm{cm^2\,V^{-1}\,s^{-1}}$ at 300 K, and it decreased below 200 K, reflecting VRH conduction, and reached $\sim 0.01\,\mathrm{cm^2\,V^{-1}\,s^{-1}}$ at 150 K. We suggest that the interaction between itinerant hole carriers and localized magnetic moment is responsible for the modulation of negative MR across MIT. On the other hand, the fact that dominant charge carriers are holes is surprising, given the broad bandwidth of the early transition-metal oxides.

To reveal the nature of the HT metallic and LT insulating phases, we performed synchrotron radiation PES across the MIT. Figure 5(a) shows the temperature dependence of valence-band spectra for the CsW_2O_6 film. The density of states (DOS) around 14–10 eV was derived from the Cs 5p states, whose spectral shape changed with temperatures, which will be discussed later together with the peak split of Cs 4d core levels. The broad DOS around 10–4 eV is mainly composed of the O 2p states, as it is common for other metal oxides [29]. The spectral shape of the O 2p states was slightly different between the HT (300 K) and LT (120 and 40 K) phases, reflecting the occurrence of the MIT associated with charge disproportionation. The small DOS near E_F is associated with the W 5d states. In order to see the change of W 5d states between the HT and LT phases in detail, the magnification near E_F is shown in the inset of Fig. 5(a). In the HT phase, a small but finite DOS was found at E_F, which was a sign of metallic nature. In contrast, in the LT phase, a clear gap opened near E_F, which verified the insulating nature. These spectral features near E_F indicate the MIT from the viewpoint of the electronic ground states and support the magnetotransport properties.

Figure 5(b) shows the temperature dependence of the W 4f core-level spectra. The W 4f core levels split into two peaks owing to spin-orbit interaction. The peaks centered at 36.5 (38.5) eV were assigned to the $J = 7/2$ (5/2) states. With decreasing the temperature, the slight peak shift of the main peak and evolution of the shoulder structures at the lower binding-energy side were clearly observed. To analyze the spectral shape in detail, we deconvoluted the W 4f core-level spectra using Voigt functions. The raw spectra, fitting results, and each component are separately indicated in Fig. 5(c). (See the details of the fitting in the Supplemental Material [30].) In the HT phase (300 K), the W 4f core-level spectrum was well fitted by only a single component, suggesting the delocalization of hole carriers residing in the W 5d state. Therefore, we tentatively assigned this profile to a $W^{5.5+}$ state and used it as a reference for the following analysis. In contrast to the HT phase, W 4f core-level spectra for the LT phase (40 and 120 K) could not be fitted by another single component alone, but excess spectral weight could be derived from an additional small component at the lower binding-energy side as seen in Fig. 5(b). The main component appeared at slightly higher binding energy compared with the reference $W^{5.5+}$ state. Although all the spectral features would have been smeared (to some extent) due to the surface oxidation layer and/or surface adsorbates, a chemical shift between those two components of 1.2 eV coincides with that between W^{6+} and W^{5+} states [31–33]. Therefore, we assigned

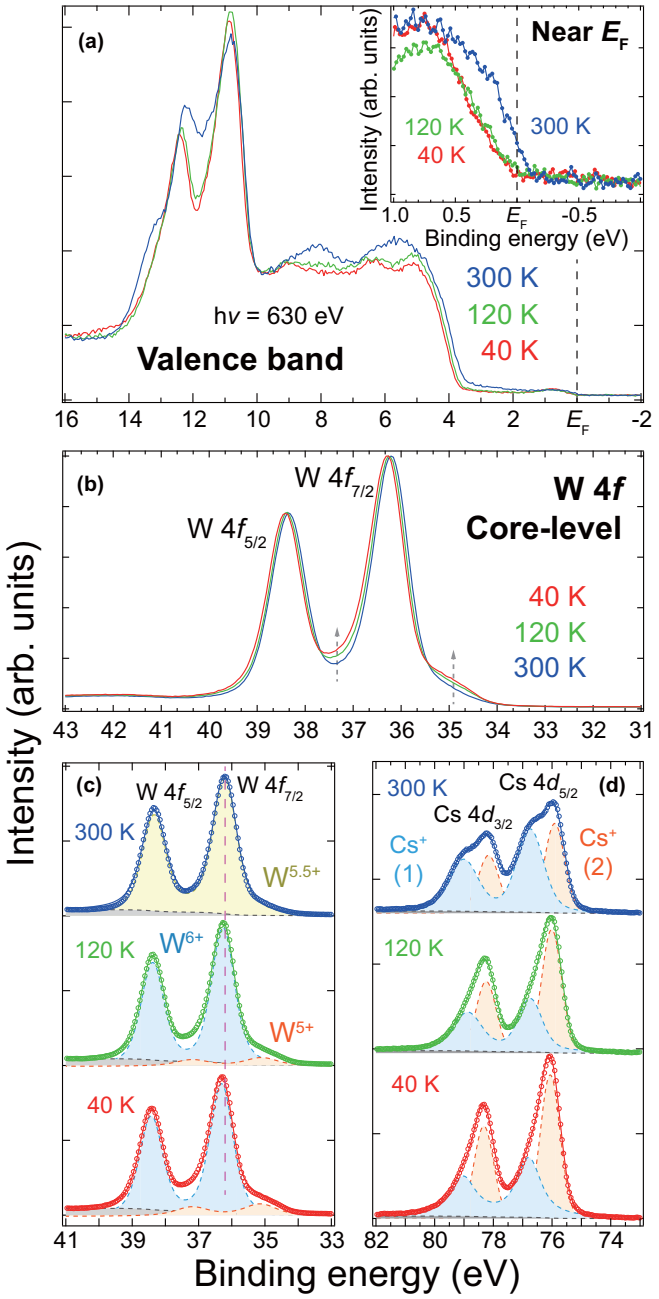

FIG. 5. (a) Valence-band, (b), (c) W 4f core-level, and (d) Cs 4d core-level spectra of CsW_2O_6 films taken at 40, 120, and 300 K. The magnification near E_F is shown in the inset of (a). The open markers, solid lines, and broken curves in (c) and (d) represent raw spectra, fitting curves, and each component in core-level fitting, respectively.

the main and small components to W^{6+} and W^{5+} states, respectively.

The spectral evolution of W 4f core levels suggests that the charge disproportionation from $W^{5.5+}$ to W^{6+} and W^{5+} occurs across the HT to LT phase transition. In fact, the $W^{5.5+}$ state was located in the middle of the W^{6+} and W^{5+} states as indicated by the vertical broken line in Fig. 5(b). Such charge disproportionation and resultant spectral change are also reported for spinel-type $CuIr_2S_4$ [20,34]. $CuIr_2S_4$ with the pyrochlore lattice has $5d^{5.5}$ states ($Ir^{3.5+}$) with a low-spin configuration, which is electron-hole symmetry to $5d^{0.5}$ ($W^{5.5+}$) of CsW_2O_6 in the degenerated t_{2g} state. The single component ($Ir^{3.5+}$) of the Ir 4f core-level spectrum split into two components (Ir^{3+} and Ir^{4+}) below 226 K, where the MIT occurred.

Figure 5(d) shows the temperature dependence of the Cs 4d core-level spectra. Cs 4d core levels also split into two peaks owing to spin-orbit interactions. The peaks around 76 (78.5) eV were assigned to the $J = 5/2$ (3/2) states of Cs 4d core levels. Interestingly, their spectral shape drastically changed across the MIT despite the core levels of electronically inert alkali ion. Both Cs 4d core-level spectra for the LT phase (40 and 120 K) were quite similar, suggesting that the spectral evolution did not merely follow decreasing temperature but associated with the MIT. To interpret anomalous spectral evolution, we also deconvoluted the Cs 4d core levels using Voigt functions. All the spectra were well fitted by two components assigned to Cs^+ (1) and Cs^+ (2) states. In the HT phase (300 K), the peak intensity of each component was comparable to the other. In contrast, those for the LT phase were significantly different from each other. We presume that the Cs^+ (1) and Cs^+ (2) states are derived from the Cs^+ cations located at two different sites in the large cages surrounded by the octahedral WO_6 framework. The chemical shift of the Cs 4d core levels in principle arises from degree of core-hole screening of Cs^+ cations. The Cs^+ cations located at the farther (nearer) sites with respect to the cage W and O atoms would affect the smaller (larger) screening effects, resulting in the higher (lower) binding energy of the Cs 4d core level.

In the cubic β-pyrochlore lattice, A^+ cations in the large cages are known to change location, leading to a rattling motion and multisites occupation, as illustrated in Fig. 1(b) [4]. In the HT phase of our sample, the Cs^+ cations likely occupy both Cs^+ (1) and Cs^+ (2) sites according to the rattling motion. On the other hand, Cs^+ cations may favor the nearer Cs^+ (2) sites in the LT phase owing to a partial suppression of the rattling motion associated with structural deformation from cubic to orthorhombic. Actually, it is revealed from the Rietveld analysis of powder x-ray and neutron diffractions that the Debye-Waller factor of the Cs atom significantly decreases in comparison with that of W and O atoms in the LT phase [9]. Furthermore, similar anomalous core-level spectra of rattling atoms are reported for cage materials [35–38], including a rattling superconducting material of $Ba_{24}Ge_{100}$, where the 12d-site Ba exists inside of the large cage of Ge. The 12d-site Ba 4d core levels split into two components (12d-1 and 12d-2) at 300 K reflecting the rattling motion. Moreover, their intensity ratio changes involving the lattice distortion at 20 K [35].

We discuss the aforementioned results to shed light on the MIT and bad metallicity of the HT phase ($d\rho/dT < 0$). Figure 6 shows the schematic illustration of the MIT in β-pyrochlore-type-CsW_2O_6. The bad metallicity in the HT phase is previously ascribed to poor crystallinity [9], and should now be considered as an intrinsic property of CsW_2O_6. The negative MR lasting even at 300 K is a clear indication of a correlated metal, where charge and/or spin fluctuations cause carrier scattering. In addition, rattling cations may

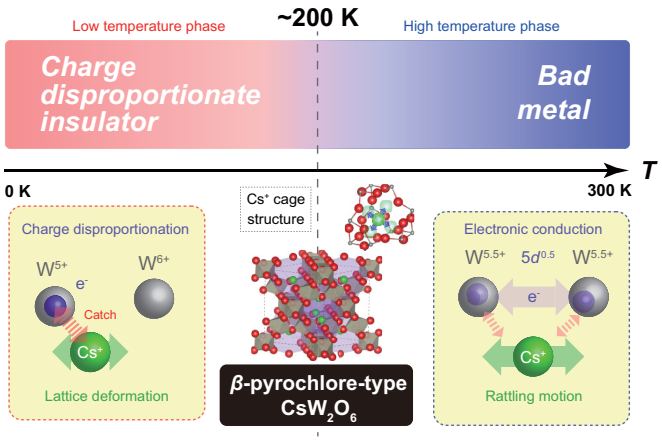

FIG. 6. Schematic illustration of the metal-insulator transition in β-pyrochlore-type-CsW_2O_6. The transition is associated with charge disproportionation of $W^{5.5+}$ and rattling motion of Cs^+.

interact with itinerate carries in the cages by Coulomb interaction [4]. The charge disproportionation at the W site and suppression of the rattling motion of Cs^+ cations in the LT phase manifest themselves across the MIT, which involves the cubic-to-orthorhombic transition in bulk. As discussed in the Cs 4*d* core-level spectra [Fig. 5(d)], Cs^+ cations tend to be located near the edge of the cage in the LT phase, which can strongly interact with the W 5*d* electrons, resulting in the charge disproportionate insulating states. Recent study for a rattling material of $Cu_{12}Sb_4S_{13}$ reveals that the MIT involving structural transition is attributed to Cu rattling displacements, and vice versa [39]. Therefore, manipulation of the rattling motion and charge disproportionate states of CsW_2O_6 is expected to influence MIT and even lead to the emergence of unprecedented electronic phases. It has been recently pointed out that CsW_2O_6 can be superconducting upon suppressing the carrier localization [40]. Metallic and superconducting ground states are actually stabilized by applying high pressure or substitutional carrier doping in materials closely related to CsW_2O_6 ($Cu_{12}Sb_4S_{13}$ [41] and $CuIr_2S_4$ [42]). Furthermore, because of thin film form, epitaxial strain and ionic liquid-gated carrier accumulation, which were recently developed as powerful tools for controlling physical properties, were also usable. Using these advanced techniques, the LT insulating phase could be suppressed and exotic electronic phases would be induced in CsW_2O_6.

IV. CONCLUSION

In summary, we have successfully grown single-crystalline β-pyrochlore-type CsW_2O_6 epitaxial films on YSZ (111) substrates using the PLD technique. The temperature dependence of resistivity clearly indicated the phase transition at 200 K. The HT phase exhibited rather insulating behavior in the temperature dependence of resistivity, indicating intrinsic bad metallicity. The magnetotransport measurements revealed negative magnetoresistances and positive Hall coefficient in both LT and HT phases. It was revealed from PES measurements that the valence band spectra indicated DOS at E_F in the HT metallic phase, which vanished in the LT insulating phase. The W 4*f* core-level spectrum changed its shape across the MIT, where two components were clearly discriminated in the insulating phase, suggesting the charge disproportionation of W^{5+} and W^{6+}. The Cs 4*d* core-level spectrum also drastically changed its spectral shape involving the MIT, reflecting the rattling motion of Cs^+ cations. The magnetotransport and photoemission measurements strongly suggest that CsW_2O_6 is the first material, which shows the charge disproportionate MIT associated with rattling motion.

ACKNOWLEDGMENTS

This work was partly supported by MEXT Elements Strategy Initiative to Form Core Research Center and a Japan Society for the Promotion of Science (JSPS) Grant-in-Aid for Scientific Research (No. 16H05983, No. 18H03925, and No. 18J10171). The work at KEK-PF was done under the approval of the Program Advisory Committee (Proposals No. 2017G596 and No. 2015S2-005) at the Institute of Materials Structure Science, KEK. T. S. acknowledges the financial support from a JSPS Research Fellowship for Young Scientists.

[1] E. Shoko, Y. Okamoto, G. J. Kearley, V. K. Peterson, and G. J. Thorogood, Novel K rattling: A new route to thermoelectric materials? J. Appl. Phys. **115**, 033703 (2014).

[2] M. Yoshida, K. Arai, R. Kaido, M. Takigawa, S. Yonezawa, Y. Muraoka, and Z. Hiroi, NMR Observation of Rattling Phonons in the Pyrochlore Superconductor KOs_2O_6, Phys. Rev. Lett. **98**, 197002 (2007).

[3] T. Shimojima, Y. Shibata, K. Ishizaka, T. Kiss, A. Chainani, T. Yokoya, T. Togashi, X. -Y. Wang, C. T. Chen, S. Watanabe, J. Yamaura, S. Yonezawa, Y. Muraoka, Z. Hiroi, T. Saitoh, and S. Shin, Interplay of Superconductivity and Rattling Phenomena in β;-Pyrochlore KOs_2O_6 Studied by Photoemission Spectroscopy, Phys. Rev. Lett. **99**, 117003 (2007).

[4] Z. Hiroi, J. Yamaura, and K. Hattori, Rattling good superconductor: β;-Pyrochlore oxides AOs_2O_6, J. Phys. Soc. Jpn. **81**, 011012 (2012).

[5] M. A. Subramanian, G. Aravamudan, and G. V. S. Rao, Oxide pyrochlores — A review, Prog. Solid State Chem. **15**, 55 (1983).

[6] G. J. Snyder and E. S. Toberer, Complex thermoelectric materials, Nat. Mater. **7**, 105 (2008).

[7] M. Christensen, A. B. Abrahamsen, N. B. Christensen, F. Juranyi, N. H. Andersen, K. Lefmann, J. Andreasson, C. R. H. Bahl, and B. B. Iversen, Avoided crossing of rattler modes in thermoelectric materials, Nat. Mater. **7**, 811 (2008).

[8] R. J. Cava, R. S. Roth, T. Siegrist, B. Hessen, J. J. Krajewski, and W. F. Peck, Jr., $Cs_{8.5}W_{15}O_{48}$ and CsW_2O_6: Members of a new homologous series of cesium tungsten oxides, J. Solid State Chem. **103**, 359 (1993).

[9] D. Hirai, M. Bremholm, J. M. Allred, J. Krizan, L. M. Schoop, Q. Huang, J. Tao, and R. J. Cava, Spontaneous Formation of Zigzag Chains at the Metal-Insulator Transition in the β;-Pyrochlore CsW_2O_6, Phys. Rev. Lett. **110**, 166402 (2013).

[10] Y. Machida, S. Nakatsuji, S. Onoda, T. Tayama, and T. Sakakibara, Time-reversal symmetry breaking and spontaneous Hall effect without magnetic dipole order, Nature (London) **463**, 210 (2010).

[11] X. Wan, A. M. Turner, A. Vishwanath, and S. Y. Savrasov, Topological semimetal and Fermi-arc surface states in the electronic structure of pyrochlore iridates, Phys. Rev. B **83**, 205101 (2011).

[12] T. Kondo, M. Nakayama, R. Chen, J. J. Ishikawa, E. -G. Moon, T. Yamamoto, Y. Ota, W. Malaeb, H. Kanai, Y. Nakashima, Y. Ishida, R. Yoshida, H. Yamamoto, M. Matsunami, S. Kimura, N. Inami, K. Ono, H. Kumigashira, S. Nakatsuji, L. Balents, and S. Shin, Quadratic Fermi node in a 3D strongly correlated semimetal, Nat. Commun. **6**, 10042 (2015).

[13] Z. Tian, Y. Kohama, T. Tomita, H. Ishizuka, T. H. Hsieh, J. J. Ishikawa, K. Kindo, L. Balents, and S. Nakatsuji, Field-induced quantum metal–insulator transition in the pyrochlore iridate $Nd_2Ir_2O_7$, Nat. Phys. **12**, 134 (2016).

[14] T. Oshima, K. Yokoyama, M. Niwa, and A. Ohtomo, Pulsed-laser deposition of superconducting $LiTi_2O_4$ ultrathin films, J. Cryst. Growth **419**, 153 (2015).

[15] T. Soma, K. Yoshimatsu, and A. Ohtomo, Epitaxial growth of hexagonal tungsten bronze Cs_xWO_3 films in superconducting phase region exceeding bulk limit, Appl. Phys. Express **9**, 075801 (2016).

[16] T. H. Etsell and S. N. Flengas, The electrical properties of solid oxide electrolytes, Chem. Rev. **70**, 339 (1970).

[17] S. Yonezawa, Y. Muraoka, Y. Matsushita and Z. Hiroi, Superconductivity in a pyrochlore-related oxide KOs_2O_6, J. Phys.: Condens. Matter **16**, L9 (2004).

[18] T. C. Fujita, Y. Kozuka, M. Uchida, A. Tsukazaki, T. Arima, and M. Kawasaki, Odd-parity magnetoresistance in pyrochlore iridate thin films with broken time-reversal symmetry, Sci. Rep. **5**, 9711 (2015).

[19] J. C. Gallagher, B. D. Esser, R. Morrow, S. R. Dunsiger, R. E. A. Williams, P. M. Woodward, D. W. McComb, and F. Y. Yang, Epitaxial growth of iridate pyrochlore $Nd_2Ir_2O_7$ films, Sci. Rep. **6**, 22282 (2016).

[20] P. G. Radaelli, Y. Horibe, M. J. Gutmann, H. Ishibashi, C. H. Chen, R. M. Ibberson, Y. Koyama, Y. -S. Hor, V. Kiryukhin, and S. -W. Cheong, Formation of isomorphic Ir^{3+} and Ir^{4+} octamers and spin dimerization in the spinel $CuIr_2S_4$, Nature (London) **416**, 155 (2002).

[21] L. L. Fan, S. Chen, Z. L. Luo, Q. H. Liu, Y. F. Wu, L. Song, D. X. Ji, P. Wang, W. S. Chu, C. Gao, C. W. Zou, and Z. Y. Wu, Strain dynamics of ultrathin VO_2 film grown on TiO_2 (001) and the associated phase transition modulation, Nano Lett. **14**, 4036 (2014).

[22] J. Sakai, P. Limelette, and H. Funakubo, Transport properties and c/a ratio of V_2O_3 thin films grown on C- and R-plane sapphire substrates by pulsed laser deposition, Appl. Phys. Lett. **107**, 241901 (2015).

[23] J. J. Ishikawa, E. C. T. O'Farrell, and S. Nakatsuji, Continuous transition between antiferromagnetic insulator and paramagnetic metal in the pyrochlore iridate $Eu_2Ir_2O_7$, Phys. Rev. B **85**, 245109 (2012).

[24] Y. J. Chang, C. H. Kim, S. -H. Phark, Y. S. Kim, J. Yu, and T. W. Noh, Fundamental Thickness Limit of Itinerant Ferromagnetic $SrRuO_3$, Phys. Rev. Lett. **103**, 057201 (2009).

[25] M. Huijben, L. W. Martin, Y. -H. Chu, M. B. Holcomb, P. Yu, G. Rijnders, D. H. A. Blank, and R. Ramesh, Critical thickness and orbital ordering in ultrathin $La_{0.7}Sr_{0.3}MnO_3$, Phys. Rev. B **78**, 094413 (2008).

[26] R. Scherwitzl, S. Gariglio, M. Gabay, P. Zubko, M. Gibert, and J. -M. Triscone, Metal-Insulator Transition in Ultrathin $LaNiO_3$ Films, Phys. Rev. Lett. **106**, 246403 (2011).

[27] V. Ambegaokar, B. I. Halperin, and J. S. Langer, Hopping conductivity in disordered systems, Phys. Rev. B **4**, 2612 (1971).

[28] D. Singh, C. S. Yadav, and B. Viswanath, Magnetoresistance across metal-insulator transition in VO_2 micro crystals, Mater. Lett. **196**, 248 (2017).

[29] R. Eguchi, M. Taguchi, M. Matsunami, K. Horiba, K. Yamamoto, Y. Ishida, A. Chainani, Y. Takata, M. Yabashi, D. Miwa, Y. Nishino, K. Tamasaku, T. Ishikawa, Y. Senba, H. Ohashi, Y. Muraoka, Z. Hiroi, and S. Shin, Photoemission evidence for a Mott-Hubbard metal-insulator transition in VO_2, Phys. Rev. B **78**, 075115 (2008).

[30] See Supplemental Material at http://link.aps.org/supplemental/10.1103/PhysRevMaterials.2.115003 for details of fitting of W $4f$ core-level spectra.

[31] G. Li, S. Zhang, C. Guo, and S. Liu, Absorption and electrochromic modulation of near-infrared light: Realized by tungsten suboxide, Nanoscale **8**, 9861 (2016).

[32] S. Cong, Y. Yuan, Z. Chen, J. Hou, M. Yang, Y. Su, Y. Zhang, L. Li, Q. Li, F. Geng, and Z. Zhao, Noble metal-comparable SERS enhancement from semiconducting metal oxides by making oxygen vacancies, Nat. Commun. **6**, 7800 (2015).

[33] L. Yang, B. Liu, T. Liu, X. Ma, H. Li, S. Yin, T. Sato, and Y. Wang, A $P25/(NH_4)_xWO_3$ hybrid photocatalyst with broad spectrum photocatalytic properties under UV, visible, and near-infrared irradiation, Sci. Rep. **7**, 45715 (2017).

[34] K. Takubo, S. Hirata, J.-Y. Son, J. W. Quilty, T. Mizokawa, N. Matsumoto, and S. Nagata, X-Ray Photoemission Study of $CuIr_2S_4$: $Ir^{3+}-Ir^{4+}$ Charge Ordering and the Effect of Light Illumination, Phys. Rev. Lett. **95**, 246401 (2005).

[35] J. Tang, J. Xu, S. Heguri, H. Fukuoka, S. Yamanaka, K. Akai, and K. Tanigaki, Electron-Phonon Interactions of Si_{100} and Ge_{100} Superconductors with Ba Atoms Inside, Phys. Rev. Lett. **105**, 176402 (2010).

[36] T. Rachi, M. Kitajima, K. Kobayashi, F. Guo, T. Nakano, Y. Ikemoto, K. Kobayashi, and K. Tanigaki, Soft x-ray spectroscopy of $Ba_{24}Ge_{100}$: Electronic phase transition and Ba-atom rattling, J. Chem. Phys. **123**, 074503 (2005).

[37] J. Tang, Z. Li, J. Ju, R. Kumashiro, M. A. Avila, K. Suekuni, T. Takabatake, F. Guo, K. Kobayashi, K. Akai, and K. Tanigaki, Soft x-ray photoelectron spectroscopy study of type-I clathrates, Sci. Technol. Adv. Mater. **9**, 044207 (2008).

[38] T. Wakita, E. Paris, T. Mizokawa, M. Y. Hacisalihoğlu, K. Terashima, H. Okazaki, O. Proux, I. Kieffer, E. Lahera, W. D. Net, L. Olivi, Y. Takano, Y. Muraoka, T. Yokoya, and N. L. Saini, Determination of the local structure of $CsBi_{4-x}Pb_xTe_6 (x = 0, 0.5)$ by x-ray absorption spectroscopy, Phys. Chem. Chem. Phys. **18**, 25136 (2016).

[39] A. F. May, O. Delaire, J. L. Niedziela, E. Lara-Curzio, M. A. Susner, S. L. Abernathy, M. Kirkham, and M. A. McGuire, Structural phase transition and phonon instability in $Cu_{12}Sb_4S_{13}$, Phys. Rev. B **93**, 064104 (2016).

[40] S. V. Streltsov, I. I. Mazin, R. Heid, and K.-P. Bohnen, Spin-orbit driven Peierls transition and possible exotic superconductivity in CsW_2O_6, Phys. Rev. B **94**, 241101(R) (2016).

[41] S. Kitagawa, T. Sekiya, S. Araki, T. C. Kobayashi, K. Ishida, T. Kambe, T. Kimura, N. Nishimoto, K. Kudo, and M. Nohara, Suppression of nonmagnetic insulating state by application of pressure in mineral tetrahedrite $Cu_{12}Sb_4S_{13}$, J. Phys. Soc. Jpn. **84**, 093701 (2015).

[42] G. Cao, T. Furubayashi, H. Suzuki, H. Kitazawa, T. Matsumoto, and Y. Uwatoko, Suppression of metal-to-insulator transition and appearance of superconductivity in $Cu_{1-x}Zn_xIr_2S_4$, Phys. Rev. B **64**, 214514 (2001).